

# C(sp<sup>3</sup>)–H Bond Activation by Perovskite Solar Photocatalyst Cell

Haowei Huang,<sup>†</sup> Haifeng Yuan,<sup>‡</sup> Jiwu Zhao,<sup>§</sup> Guillermo Solís-Fernández,<sup>‡</sup> Chen Zhou,<sup>||</sup> Jin Won Seo,<sup>||</sup> Jelle Hendrix,<sup>‡</sup> Elke Debroye,<sup>‡</sup> Julian A. Steele,<sup>†</sup> Johan Hofkens,<sup>‡</sup> Jinlin Long,<sup>\*,§</sup> and Maarten B. J. Roeffaers<sup>\*,†</sup>

<sup>†</sup>Department of Microbial and Molecular Systems, Centre for Surface Chemistry and Catalysis (COK), KU Leuven, Celestijnenlaan 200F, 3001 Leuven, Belgium

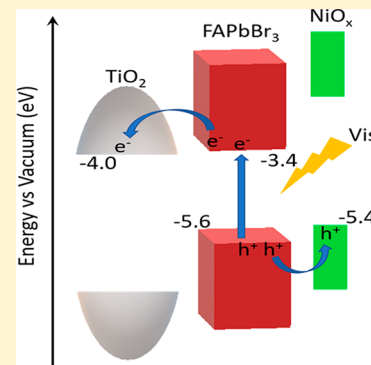
<sup>‡</sup>Department of Chemistry, Faculty of Sciences, KU Leuven, Celestijnenlaan 200F, 3001 Heverlee, Belgium

<sup>§</sup>State Key Laboratory of Photocatalysis on Energy and Environment, Fuzhou University, Fuzhou 350002, Fujian, P.R. China

<sup>||</sup>Department of Materials Engineering, KU Leuven, Kasteelpark Arenberg 44, 3001 Heverlee, Belgium

## Supporting Information

**ABSTRACT:** Inspired by efficient perovskite solar cells, we developed a three-component hybrid perovskite-based solar photocatalyst cell, NiO<sub>x</sub>/FAPbBr<sub>3</sub>/TiO<sub>2</sub>, for C(sp<sup>3</sup>)–H bond activation with high selectivity (~90%) and high conversion rates (3800 μmol g<sup>-1</sup> h<sup>-1</sup>) under ambient conditions. Time-resolved spectroscopy on our photocatalytic cell reveals efficient exciton dissociation and charge separation, where TiO<sub>2</sub> and NiO<sub>x</sub> serve as the electron- and hole-transporting layers, respectively. The photogenerated charge carriers injected into TiO<sub>2</sub> and NiO<sub>x</sub> drive the challenging C–H activation reaction via the synergetic effects of their band alignment relative to FAPbBr<sub>3</sub>. The reaction pathway is investigated by controlling the free-radical formation, and we find that C–H activation is mainly triggered by hole oxidation. Besides aromatic alkanes, also the C(sp<sup>3</sup>)–H bond in cycloalkanes can be oxidized selectively. This work demonstrates a generic strategy for engineering high-performance photocatalysts based on the perovskite solar cell concept.



Direct functionalization of saturated C–H bonds to form high value-added chemicals is one of the most challenging topics in modern chemistry. C(sp<sup>3</sup>)–H bonds are stable and thermodynamically unreactive, making their conversion into C–R bonds, like C–O, very difficult.<sup>1,2</sup> Much progress has been made in recent decades;<sup>3–5</sup> however, the process selectivity and harsh reaction conditions of current C–H activation technologies limit their widespread use.<sup>3</sup> As such, there are strong desires to develop an easy and energetically favorable route for the efficient conversion of alkanes into value-added products. Photocatalysis provides a promising solution to overcome the challenges in C–H bond activation,<sup>6</sup> with numerous semiconductors being employed for the selective photo-oxidation of C–H bonds using molecular oxygen as oxidant.<sup>7–10</sup> However, the photocatalytic performance reported until now falls short of the ideal, suffering from narrow optical absorption windows, low charge separation efficiencies, and poor product selectivity, owing to over oxidation and/or the need for specific solvents.

Organic–inorganic halide perovskites (OIHPs) typically display strong and broad light absorption and excellent charge transport properties.<sup>11</sup> These key physical characteristics suggest their application in photocatalysis within the wider context of light harvesting can be promising.<sup>12–18</sup> OIHPs can

provide a viable option for selective C–H bond activations, with previous work demonstrating FAPbBr<sub>3</sub> and CsPbBr<sub>3</sub> perovskites are useful for the selective photo-oxidation of benzylic alcohols to produce benzaldehyde.<sup>19,20</sup> The conversion rates using pure perovskite remain low because a large portion of the photogenerated charges recombine and circumvent the reaction process.

Inspired by efficient perovskite-based solar cells,<sup>21–24</sup> we set out to rationally design a more efficient perovskite photocatalyst via superior charge separation by including transporting layers for both electrons (ETL) and holes (HTL). In solar cell devices, efficient light–electricity conversions rely not only on the properties of the perovskite itself but also on the choice of both the ETL, like TiO<sub>2</sub>, and HTL, such as Spiro-OMeTAD, PEDOT, NiO<sub>x</sub>, etc.<sup>25–31</sup> With regard to choosing an effective ETL, combining FAPbBr<sub>3</sub> and CsPbBr<sub>3</sub> with TiO<sub>2</sub> provides a significant enhancement in photocatalytic benzyl alcohol oxidation.<sup>19,20</sup> Among HTL materials, we identify cheap and nontoxic p-type NiO<sub>x</sub> as a promising choice, given

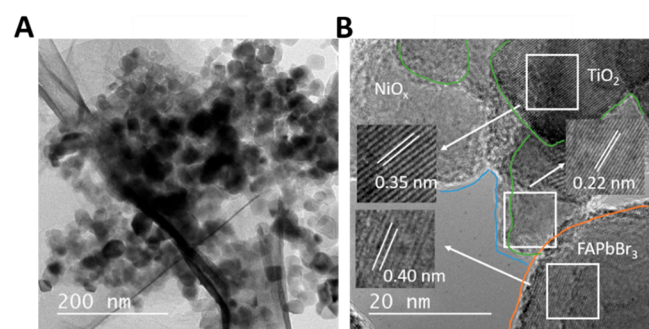
Received: September 10, 2018

Accepted: December 5, 2018

Published: December 5, 2018

its high charge carrier mobility and structural stability.<sup>31</sup> Furthermore, nickel oxides and complexes are widely used in organic synthesis like aerobic epoxidation of alkenes, oxidative dehydrogenation of alkanes to alkenes, Baeyer–Villiger oxidation and sulfoxidation, and photocatalytic organic transformation.<sup>32,33</sup> More specifically, Xiao and co-workers have shown that NiO<sub>x</sub> could extract the photogenerated holes from TiO<sub>2</sub> to enhance the oxidation of toluene to benzaldehyde.<sup>33</sup> Specifically, 2D NiO<sub>x</sub> sheets offer more coordinatively unsaturated Ni atoms, oxygen vacancies, and defect sites on the surface, being capable of stronger interactions with substrates.<sup>34</sup> Furthermore, 2D layered materials have great charge transmission capacities and are widely used in photocatalysis to lengthen the carrier lifetime.<sup>35</sup> For these reasons, adopting a similar rational design employed in solar cell devices, our final design is a three-component hybrid 2D NiO<sub>x</sub>/FAPbBr<sub>3</sub>/TiO<sub>2</sub> nanocomposite, which is capable of highly selective and efficient activation of C(sp<sup>3</sup>)–H bonds in alkanes using molecular oxygen and simulated solar light (AM1.5G).

The syntheses of NiO<sub>x</sub>, FAPbBr<sub>3</sub>, FAPbBr<sub>3</sub>/TiO<sub>2</sub>, and NiO<sub>x</sub>/FAPbBr<sub>3</sub>/TiO<sub>2</sub> are shown in the Supporting Information. X-ray diffraction (XRD) and X-ray photoelectron spectroscopy (XPS) (Figures S1–S3) results clearly indicate that FAPbBr<sub>3</sub> was prepared in its cubic phase, TiO<sub>2</sub> came as a mixed anatase–rutile phase, and NiO<sub>x</sub> was a mixture of NiOOH and Ni(OH)<sub>2</sub> with low crystallinity. A transmission electron microscopy (TEM) image of our nanocomposite is provided in Figure 1A, with a high-resolution micrograph

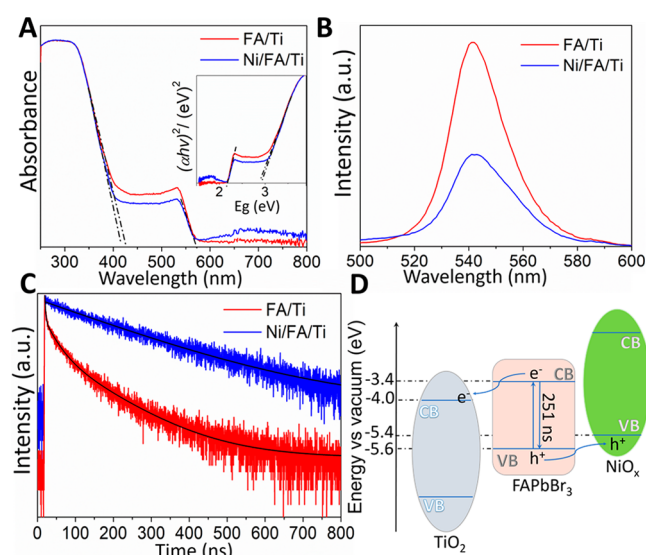


**Figure 1.** TEM (A) and HRTEM (B) images of NiO<sub>x</sub>/FAPbBr<sub>3</sub>/TiO<sub>2</sub> (Ni/FA/Ti).

(HRTEM) provided in Figure 1B. Here we see 2D NiO<sub>x</sub> sheets supporting the FAPbBr<sub>3</sub> and TiO<sub>2</sub> nanoparticles, which corresponds to the elemental mapping shown in Figure S6. In the HRTEM image, lattice fringes with 0.4, 0.35, and 0.22 nm spacing, corresponding to (011) of FAPbBr<sub>3</sub> and (101) and (001) facets of TiO<sub>2</sub>, respectively, can be identified.<sup>36,37</sup>

The optical absorption spectra of FAPbBr<sub>3</sub>/TiO<sub>2</sub> and NiO<sub>x</sub>/FAPbBr<sub>3</sub>/TiO<sub>2</sub> in Figure 2A reveal two band edges near 420 and 580 nm, which are assigned to TiO<sub>2</sub> and FAPbBr<sub>3</sub>, respectively.<sup>19</sup> Note that the absorption spectra of NiO<sub>x</sub>, TiO<sub>2</sub>, and FAPbBr<sub>3</sub> are summarized in Figure S7. Over this photonic range, NiO<sub>x</sub> barely contributes to the light absorption. A notable Urbach tail absorption could be observed in NiO<sub>x</sub>/FAPbBr<sub>3</sub>/TiO<sub>2</sub>, which is the same as that in pure NiO<sub>x</sub>, indicating dense defects.<sup>38</sup>

We next examine the photophysical processes in these materials by steady-state photoluminescence (PL) spectroscopy. FAPbBr<sub>3</sub> presents a typical PL emission around 560 nm

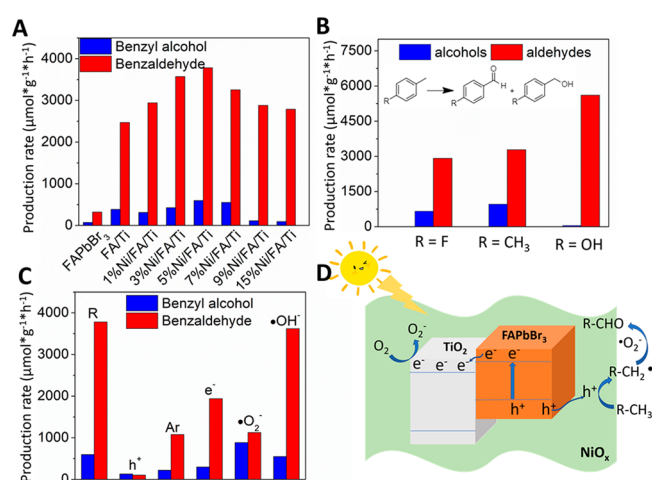


**Figure 2.** UV–vis DRS spectra (A) with the corresponding band gaps shown in the inset, steady-state PL spectra (B) and PL decay spectra (C) of the prepared FAPbBr<sub>3</sub>/TiO<sub>2</sub> (FA/Ti) and 5% NiO<sub>x</sub>/FAPbBr<sub>3</sub>/TiO<sub>2</sub> (Ni/FA/Ti), and (D) experimentally supported mechanistic energy diagram of photoinduced charge transfer in NiO<sub>x</sub>/FAPbBr<sub>3</sub>/TiO<sub>2</sub>.

(Figure S8). Addition of NiO<sub>x</sub> and TiO<sub>2</sub> induces a blue shift in the FAPbBr<sub>3</sub> PL spectra, with a peak at 540 nm in both NiO<sub>x</sub>/FAPbBr<sub>3</sub>/TiO<sub>2</sub> and FAPbBr<sub>3</sub>/TiO<sub>2</sub> (Figure 2B), associated with the significantly smaller size of the FAPbBr<sub>3</sub> nanocrystals obtained in these composites.<sup>19</sup> We note that PL intensity is strongly quenched after the addition of NiO<sub>x</sub> onto FAPbBr<sub>3</sub>/TiO<sub>2</sub>, indicating improved charge separation and reduced radiative recombination.<sup>14,39</sup> Time-resolved photoluminescence (TRPL) decays in Figure 2C reveal significant changes in charge dynamics in the hybrid system. Three exponential components are required to fit the FAPbBr<sub>3</sub>/TiO<sub>2</sub> TRPL decay in Figure 2C, being linked to (1) trap-assisted exciton recombination ( $\tau_1 = 2.2$  ns), (2) exciton recombination ( $\tau_2 = 31.2$  ns), and (3) free-carrier recombination ( $\tau_3 = 136$  ns). For completeness, a complete list of parameters used is depicted in Table S1.<sup>19,40</sup> Interestingly, the introduction of NiO<sub>x</sub> not only strongly reduces the PL intensity but also reshapes the TRPL decay into a monoexponential decay with a single lifetime value of 251 ns related to free-carrier recombination ( $\tau_3$ ). Moreover, the lifetime of free carriers in NiO<sub>x</sub>/FAPbBr<sub>3</sub>/TiO<sub>2</sub> is nearly doubled. These findings provide clear evidence for the strong suppression of excitonic recombinations through effective charge separation and balanced hole/electron extraction from FAPbBr<sub>3</sub> to the NiO<sub>x</sub> and TiO<sub>2</sub> layers.<sup>19,41,42</sup> First, because of the relative band alignment of the three materials—NiO<sub>x</sub>, perovskite, and TiO<sub>2</sub>—the charge separation is much improved at the material interfaces. This exact mechanism is of course exploited in the efficient application of perovskite-based photovoltaics. The efficient charge separation thus leads to a significantly reduced exciton population, followed by the suppression of their radiative contributions. Second, besides the separation of excitonic charges at the interfaces, the free electrons and holes are also extracted by NiO<sub>x</sub> and TiO<sub>2</sub> for the same reasons of their band alignments relative to the absorbing perovskite. As a consequence of the extraction of charges from the perovskite material to NiO<sub>x</sub> and TiO<sub>2</sub>, the overall density of charges on

the perovskite that are available for charge recombination reduces, resulting in much lower PL emission intensity. Furthermore, as the free-carrier population is reduced, promoting a longer time for free carriers to encounter each other and radiatively recombine, the PL decay time becomes longer on average, i.e., lower free-carrier population. These findings reveal the efficient separation and extraction pathways for photogenerated charge carriers in the hybrid photocatalyst materials: excitons and free carriers are generated in FAPbBr<sub>3</sub> after photon absorption, and the favorable band alignments of the HTL and ETL efficiently separate and extract electrons and holes from the perovskite, suppressing excitonic PL emissions.

Next, we tested our photocatalysts for the selective photo-oxidation of C(sp<sup>3</sup>)-H of the methyl group in toluene (Tol) saturated with O<sub>2</sub> and simulated solar light (AM1.5G) at room temperature. The photocatalytic performance under solar light irradiation is summarized in Figures 3A and S9. GC-MS was



**Figure 3.** (A) Photocatalytic oxidation of C(sp<sup>3</sup>)-H in Tol over pure FAPbBr<sub>3</sub>, FAPbBr<sub>3</sub>/TiO<sub>2</sub>, and a series of NiO<sub>x</sub>/FAPbBr<sub>3</sub>/TiO<sub>2</sub> (Ni/FA/Ti) hybrids. (B) Photocatalytic oxidation of C(sp<sup>3</sup>)-H in substituted toluenes over 5% NiO<sub>x</sub>/FAPbBr<sub>3</sub>/TiO<sub>2</sub>. (C) C(sp<sup>3</sup>)-H Tol oxidation in the absence or presence of various radical scavengers. (D) Corresponding schematic of the proposed selective photocatalytic conversion of Tol to BD over the NiO<sub>x</sub>/FAPbBr<sub>3</sub>/TiO<sub>2</sub>. The detailed reaction scheme can be found in the Supporting Information. Reaction conditions: photocatalysts (0.01 g), Tol (2.5 mL) saturated with O<sub>2</sub>, AM1.5G simulated light irradiation (85 mW/cm<sup>2</sup>), and irradiation time (4 h).

used to check the products, as shown in Figure S10. After 4 h of illumination, the formation rates of benzaldehyde (BD) were 320 and 1129 μmol h<sup>-1</sup> g<sup>-1</sup>, respectively, for FAPbBr<sub>3</sub> and TiO<sub>2</sub>. Additionally, significant amounts of benzyl alcohol (BA) as a side product are produced: 54 and 72 μmol h<sup>-1</sup> g<sup>-1</sup> respectively, resulting in Tol oxidation selectivity to benzaldehyde of 81% for pure FAPbBr<sub>3</sub> and 95% for pure TiO<sub>2</sub>. Comparing 15 wt % FAPbBr<sub>3</sub>/TiO<sub>2</sub> with FAPbBr<sub>3</sub>, TiO<sub>2</sub> as ETL results in about 8-fold improved production rates for BD (2470 μmol h<sup>-1</sup> g<sup>-1</sup>) and BA (387 μmol h<sup>-1</sup> g<sup>-1</sup>). Further integration of an HTL (NiO<sub>x</sub>), to prepare a NiO<sub>x</sub>/FAPbBr<sub>3</sub>/TiO<sub>2</sub> solar photocatalyst cell, improved the initial activity of FAPbBr<sub>3</sub> up to 12 times. The best photocatalytic activity is achieved with 5 wt % NiO<sub>x</sub> loading with an impressive Tol oxidation rate of 3800 μmol h<sup>-1</sup> g<sup>-1</sup> to BD and 0.25% external quantum efficiency at 400 nm. The yield of BD is 0.73% (see Table S3). Note that further increasing NiO<sub>x</sub> loadings beyond

5 wt % leads to diminishing returns, with reduced conversions driven by competitive light absorption. The optimal 5 wt % NiO<sub>x</sub> loading is also found to improve the conversion selectivity to BD to 86%. Control experiments using pure NiO<sub>x</sub>, NiO<sub>x</sub>/FAPbBr<sub>3</sub>, and NiO<sub>x</sub>/TiO<sub>2</sub> are further compared in Figures S9 and S11. Similar performances (Figure S12) were obtained using purely visible light (>420 nm). However, the photocatalytic reaction by using visible light shows a lower production rate that is 10 times less than that obtained with solar light. This indicates that with solar light irradiation, UV photons can be harvested by TiO<sub>2</sub> to generate holes and electrons and react with Tol.

The remarkable activity for the selective photocatalytic oxidation of C(sp<sup>3</sup>)-H in Tol offered by the three-component photocatalyst was also confirmed with several substituted toluenes in the conversion to the corresponding aldehydes (Figure 3B), which proves the universality of the strategy reported here. The conversion rates for *p*-fluorobenzaldehyde, *p*-methylbenzaldehyde, and *p*-hydroxybenzaldehyde are 2915, 3280, and 5610 μmol h<sup>-1</sup> g<sup>-1</sup>, with selectivity of 81%, 77%, and 99%, respectively. The conversion, yield, and selectivity are summarized in Table S2. The material stability during repeated reaction cycles was evaluated. Figure S13 shows the results for 5 wt % NiO<sub>x</sub>/FAPbBr<sub>3</sub>/TiO<sub>2</sub> following their recycled use during five consecutive 4 h reaction cycles. After 5 cycles, the NiO<sub>x</sub>/FAPbBr<sub>3</sub>/TiO<sub>2</sub> composite retains more than 85% of its original activity. The slight loss of activity is due to the slow dissolution of FAPbBr<sub>3</sub> in the generated benzaldehyde. At the same time, water as the side product will be generated in this reaction system, which would also affect the stability of the perovskite. We remain optimistic that the design of future photocatalyst cells will ultimately resolve this problem via full encapsulation of the perovskite light harvester, i.e. the generation of a core-shell structure perovskite@HTL/ETL minimizing the contact with the more polar reaction products, and/or the use of perovskite surface passivating molecules. The photocatalyst remains active for at least five cycles, indicating that the lower limit of the turnover number (TON) is at least 263 and turnover frequency (TOF) for the first five cycles is 13.15 (h<sup>-1</sup>) (see the Supporting Information for details on the calculation). We also perform a continuous test to check the stability of our sample (see Figure S14). After 20 h of irradiation, the photocatalyst still presents a decent activity, and as the reaction time increases, the generated benzaldehyde will be further oxidized to benzoic acid.

To elucidate the exact photocatalytic reaction mechanism behind this selective oxidation reaction, we investigated in more detail the formation of free radicals that are often involved in photocatalytic organic transformation.<sup>6,25,43-45</sup> Experiments with specific radical scavengers yield more specific information regarding the role of various redox-active species, e.g., ammonium oxalate for holes, potassium persulfate for electrons, 1,4-benzoquinone for •O<sub>2</sub><sup>-</sup>, and *t*-butanol for •OH.<sup>10</sup> The effect of these specific radical scavengers on the photocatalytic Tol conversion was tested, with the findings presented in Figure 3C. In the presence of ammonium oxalate as strong hole scavenger, the Tol conversion is almost completely prohibited. Scavenging the electrons with K<sub>2</sub>S<sub>2</sub>O<sub>8</sub> reduces the Tol conversion, but it does not completely stop the reaction. A similar effect is observed when O<sub>2</sub> is replaced by Ar. Even though the Tol conversion drops in the presence of Ar and K<sub>2</sub>S<sub>2</sub>O<sub>8</sub>, the selectivity is maintained. While adding *t*-BuOH has little effect on the photocatalytic Tol oxidation, 1,4-

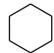
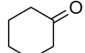

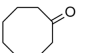


benzoquinone also leads to a reduced conversion and a higher relative BA production. Similar reactions were operated using pristine FAPbBr<sub>3</sub> (Figure S17). These free-radical scavenging experiments prove the free-radical process and highlight the vital role of the photogenerated holes to initiate the activation of Tol. These radical experiments open the door to understanding the reaction mechanism and give us an indication that the free radical is involved in this reaction. However, to obtain deeper insight into the reaction mechanism and pathway, more experiments and DFT calculations will be useful to further confirm the reaction mechanism.

Therefore, on the basis of the results of PL, TRPL, and radical experiments, we propose the following reaction mechanism in Figure 3D: (1) Visible light illumination of FAPbBr<sub>3</sub> efficiently generates charge carriers. (2) The presence of ETL (TiO<sub>2</sub>) and HTL (NiO<sub>x</sub>) efficiently separates the carries in FAPbBr<sub>3</sub>. (3) Molecular oxygen adsorbed on TiO<sub>2</sub> is reduced to ·O<sub>2</sub><sup>-</sup> with electrons, and the holes in NiO<sub>x</sub> react with Tol to form Tol radicals, a key step for the oxidation of C–H bonds. (4) These Tol radicals react with ·O<sub>2</sub><sup>-</sup> to produce the corresponding aldehyde. The generation of BA can be explained by the direct reaction of the Tol radicals with free O<sub>2</sub> dissolved in Tol to generate BA, which can be further oxidized to produce the aldehydes as well.<sup>16,17</sup>

The highly selective and efficient C(sp<sup>3</sup>)–H bond oxidation via our rationally designed perovskite solar photocatalytic cell is further tested for the activation of cycloalkanes, using again O<sub>2</sub> under simulated solar illumination (see Table 1). Our

**Table 1. Results of the Oxidation of Cycloalkanes with 5% NiO<sub>x</sub>/FAPbBr<sub>3</sub>/TiO<sub>2</sub><sup>a</sup>**

substrate	Main product	Production rate (μmol g <sup>-1</sup> h <sup>-1</sup> )	Selectivity
		89	>99%
		138	>99%

<sup>a</sup>Reaction conditions: photocatalysts (0.01 g), cycloalkanes (2.5 mL) saturated with molecular oxygen, AM1.5G simulated light irradiation (85 mW/cm<sup>2</sup>), and irradiation time (4 h).

champion 5% NiO<sub>x</sub>/FAPbBr<sub>3</sub>/TiO<sub>2</sub> displays a high activity in the selective oxidation of cyclohexane and cyclooctane, with 89 and 138 μmol h<sup>-1</sup> g<sup>-1</sup> cyclohexanone and cyclooctenone, respectively, and with >99% selectivity. The yield is 0.016% and 0.032% for cyclohexanone and cyclooctenone, respectively (see Table S4). These very promising results expand the possibilities for perovskite-based photocatalysts in organic synthesis, given that the C–H bonds in cycloalkanes are far stronger than those of aromatic methyls.

In summary, we developed a new hybrid photocatalyst inspired by the design principles expressed in the field of perovskite-based solar cells and utilized it for the highly efficient and selective functionalization of C–H bonds in alkanes under relatively mild reaction conditions. A 12-fold enhancement in Tol oxidation is achieved by loading 5 wt % NiO<sub>x</sub> onto 15% FAPbBr<sub>3</sub>/TiO<sub>2</sub>. Detailed time-resolved spectroscopy reveals the efficient photogenerated charge carrier separation in this synergistic system, and considering

the radical scavengers, a detailed reaction process for the C(sp<sup>3</sup>)–H bond activation and selective oxidation is proposed. Most importantly, this work bridges the gap between efficient photocatalyst semiconductors and well-established perovskite solar cells, which are currently a prominent feature in the field of solar energy, paving the way for the rational design of novel perovskite photocatalysts for organic synthesis.

## ■ ASSOCIATED CONTENT

### Supporting Information

The Supporting Information is available free of charge on the ACS Publications website at DOI: 10.1021/acsenerylett.8b01698.

Experimental details on materials synthesis and XPS, SEM, DRS, and photoluminescence results (PDF)

## ■ AUTHOR INFORMATION

### Corresponding Authors

\*E-mail: jllong@fzu.edu.cn.

\*E-mail: maarten.roeffaers@kuleuven.be.

### ORCID

Haifeng Yuan: 0000-0001-6652-3670

Chen Zhou: 0000-0002-4619-9014

Jin Won Seo: 0000-0003-4937-0769

Jelle Hendrix: 0000-0001-5731-1297

Julian A. Steele: 0000-0001-7982-4413

Johan Hofkens: 0000-0002-9101-0567

Jinlin Long: 0000-0002-3675-0941

Maarten B. J. Roeffaers: 0000-0001-6582-6514

### Notes

The authors declare no competing financial interest.

## ■ ACKNOWLEDGMENTS

We acknowledge financial support from the Research Foundation-Flanders (FWO, Grant Nos. G.0962.13 and G.0B49.15, doctoral fellowship to G.S.-F., and postdoctoral fellowships to H.Y. and J.A.S.), KU Leuven Research Fund (C14/15/053), the Flemish government through long-term structural funding Methusalem (CASAS2, Meth/15/04), the Hercules Foundation (HER/11/14), and the European Union (Horizon 2020) Marie Skłodowska-Curie innovation program (Grant 722591 for Ph.D. scholarship) to H.H. J.L. acknowledges the financial support of NSFC (Grant No. 21773031). J.W.S. acknowledges funding from Hercules project AKUL/13/19.

## ■ REFERENCES

- (1) Recupero, F.; Punta, C. Free Radical Functionalization of Organic Compounds Catalyzed by N-Hydroxyphthalimide. *Chem. Rev.* **2007**, *107*, 3800–3842.
- (2) Chen, M. S.; White, M. C. Combined Effects on Selectivity in Fe-catalyzed Methylene Oxidation. *Science* **2010**, *327*, 566–571.
- (3) Punniyamurthy, T.; Velusamy, S.; Iqbal, J. Recent Advances in Transition Metal Catalyzed Oxidation of Organic Substrates with Molecular Oxygen. *Chem. Rev.* **2005**, *105*, 2329–2364.
- (4) Kamata, K.; Yonehara, K.; Nakagawa, Y.; Uehara, K.; Mizuno, N. Efficient Stereo- and Regioselective Hydroxylation of Alkanes Catalyzed by a Bulky Polyoxometalate. *Nat. Chem.* **2010**, *2*, 478.
- (5) Wang, Y.; Li, H.; Yao, J.; Wang, X.; Antonietti, M. Synthesis of Boron Doped Polymeric Carbon Nitride Solids and Their Use as Metal-Free Catalysts for Aliphatic C–H Bond Oxidation. *Chem. Sci.* **2011**, *2*, 446–450.

- (6) Lang, X. J.; Chen, X. D.; Zhao, J. C. Heterogeneous Visible Light Photocatalysis for Selective Organic Transformations. *Chem. Soc. Rev.* **2014**, *43*, 473–483.
- (7) Yang, D.; Wu, T.; Chen, C.; Guo, W.; Liu, H.; Han, B. The Highly Selective Aerobic Oxidation of Cyclohexane to Cyclohexanone and Cyclohexanol over  $V_2O_5@TiO_2$  under Simulated Solar Light Irradiation. *Green Chem.* **2017**, *19*, 311–318.
- (8) Liu, Y.; Chen, L.; Yuan, Q.; He, J.; Au, C.-T.; Yin, S.-F. A Green and Efficient Photocatalytic Route for the Highly-Selective Oxidation of Saturated Alpha-Carbon C–H Bonds in Aromatic Alkanes Over Flower-Like  $Bi_2WO_6$ . *Chem. Commun.* **2016**, *52*, 1274–1277.
- (9) Zhang, P. F.; Wang, Y.; Yao, J.; Wang, C. M.; Yan, C.; Antonietti, M.; Li, H. R. Visible-Light-Induced Metal-Free Allylic Oxidation Utilizing a Coupled Photocatalytic System of G-C<sub>3</sub>N<sub>4</sub> and N-Hydroxy Compounds. *Adv. Synth. Catal.* **2011**, *353*, 1447–1451.
- (10) Zhang, Y. H.; Zhang, N.; Tang, Z. R.; Xu, Y. J. Transforming Cds into an Efficient Visible Light Photocatalyst for Selective Oxidation of Saturated Primary C–H Bonds Under Ambient Conditions. *Chem. Sci.* **2012**, *3*, 2812–2822.
- (11) Gao, P.; Gratzel, M.; Nazeeruddin, M. K. Organohalide Lead Perovskites for Photovoltaic Applications. *Energy Environ. Sci.* **2014**, *7*, 2448–2463.
- (12) Wu, Y. Q.; Wang, P.; Zhu, X. L.; Zhang, Q. Q.; Wang, Z. Y.; Liu, Y. Y.; Zou, G. Z.; Dai, Y.; Whangbo, M. H.; Huang, B. B. Composite of  $CH_3NH_3PbI_3$  with Reduced Graphene Oxide as a Highly Efficient and Stable Visible-Light Photocatalyst for Hydrogen Evolution in Aqueous HI Solution. *Adv. Mater.* **2018**, *30*, 1704342.
- (13) Park, S.; Chang, W. J.; Lee, C. W.; Park, S.; Ahn, H. Y.; Nam, K. T. Photocatalytic Hydrogen Generation from Hydriodic Acid Using Methylammonium Lead Iodide in Dynamic Equilibrium with Aqueous Solution. *Nat. Energy* **2017**, *2*, 16185.
- (14) Xu, Y. F.; Yang, M. Z.; Chen, B. X.; Wang, X. D.; Chen, H. Y.; Kuang, D. B.; Su, C. Y. A  $Cspbbr_3$  Perovskite Quantum Dot/Graphene Oxide Composite for Photocatalytic  $CO_2$  Reduction. *J. Am. Chem. Soc.* **2017**, *139*, 5660–5663.
- (15) Chen, K.; Deng, X. H.; Dodekatos, G.; Tuysuz, H. Photocatalytic Polymerization of 3, 4-Ethylenedioxythiophene over Cesium Lead Iodide Perovskite Quantum Dots. *J. Am. Chem. Soc.* **2017**, *139*, 12267–12273.
- (16) Xu, Y.-F.; Wang, X.-D.; Liao, J.-F.; Chen, B.-X.; Chen, H.-Y.; Kuang, D.-B. Amorphous- $TiO_2$ -Encapsulated  $Cspbbr_3$  Nanocrystal Composite Photocatalyst with Enhanced Charge Separation and  $CO_2$  Fixation. *Adv. Mater. Interfaces* **2018**, *5*, 1801015.
- (17) Xu, Y.-F.; Yang, M.-Z.; Chen, H.-Y.; Liao, J.-F.; Wang, X.-D.; Kuang, D.-B. Enhanced Solar-Driven Gaseous  $CO_2$  Conversion by  $Cspbbr_3$  Nanocrystal/Pd Nanosheet Schottky-Junction Photocatalyst. *ACS Appl. Energy Mater.* **2018**, *1*, 5083–5089.
- (18) Zhou, L.; Xu, Y.-F.; Chen, B.-X.; Kuang, D.-B.; Su, C.-Y. Synthesis and Photocatalytic Application of Stable Lead-Free  $Cs_2AgBiBr_6$  Perovskite Nanocrystals. *Small* **2018**, *14*, 1703762.
- (19) Huang, H.; Yuan, H.; Janssen, K. P. F.; Solís-Fernández, G.; Kuang, Y.; Tan, C. Y. X.; Jonckheere, D.; Debroye, E.; Long, J.; Hendrix, J.; et al. Efficient and Selective Photocatalytic Oxidation of Benzylic Alcohols with Hybrid Organic–Inorganic Perovskite Materials. *ACS Energy Lett.* **2018**, *3*, 755–759.
- (20) Schünemann, S.; Van Gestel, M.; Tüysüz, H. A  $CsPbBr_3/TiO_2$  Composite for Visible-Light Driven Photocatalytic Benzyl Alcohol Oxidation. *ChemSusChem* **2018**, *11*, 2057.
- (21) Brenner, T. M.; Egger, D. A.; Kronik, L.; Hodes, G.; Cahen, D. Hybrid Organic–Inorganic Perovskites: Low-cost Semiconductors with Intriguing Charge-transport Properties. *Nat. Rev. Mater.* **2016**, *1*, 150007.
- (22) Kazim, S.; Nazeeruddin, M. K.; Gratzel, M.; Ahmad, S. Perovskite as Light Harvester: a Game Changer in Photovoltaics. *Angew. Chem., Int. Ed.* **2014**, *53*, 2812–2824.
- (23) Yang, W. S.; Park, B. W.; Jung, E. H.; Jeon, N. J.; Kim, Y. C.; Lee, D. U.; Shin, S. S.; Seo, J.; Kim, E. K.; Noh, J. H.; et al. Iodide Management in Formamidinium-lead-halide–based Perovskite Layers for Efficient Solar Cells. *Science* **2017**, *356*, 1376–1379.
- (24) Tan, H. R.; Jain, A.; Voznyy, O.; Lan, X. Z.; De Arquer, F. P. G.; Fan, J. Z.; Quintero-Bermudez, R.; Yuan, M. J.; Zhang, B.; Zhao, Y. C.; et al. Efficient and Stable Solution-Processed Planar Perovskite Solar Cells via Contact Passivation. *Science* **2017**, *355*, 722–726.
- (25) Qin, P.; Tanaka, S.; Ito, S.; Tetreault, N.; Manabe, K.; Nishino, H.; Nazeeruddin, M. K.; Gratzel, M. Inorganic Hole Conductor-based Lead Halide Perovskite Solar Cells with 12.4% Conversion Efficiency. *Nat. Commun.* **2014**, *5*, 3834.
- (26) Lee, M. M.; Teuscher, J.; Miyasaka, T.; Murakami, T. N.; Snaith, H. J. Organometal Halide Perovskites Efficient Hybrid Solar Cells Based on Meso-superstructured. *Science* **2012**, *338*, 643.
- (27) Xiao, Z. G.; Bi, C.; Shao, Y. C.; Dong, Q. F.; Wang, Q.; Yuan, Y. B.; Wang, C. G.; Gao, Y. L.; Huang, J. S. Efficient, High Yield Perovskite Photovoltaic Devices Grown by Interdiffusion of Solution-processed Precursor Stacking Layers. *Energy Environ. Sci.* **2014**, *7*, 2619–2623.
- (28) Yang, Y.; Ri, K.; Mei, A. Y.; Liu, L. F.; Hu, M.; Liu, T. F.; Li, X.; Han, H. W. The Size Effect of  $TiO_2$  Nanoparticles on a Printable Mesoscopic Perovskite Solar Cell. *J. Mater. Chem. A* **2015**, *3*, 9103–9107.
- (29) Jeng, J. Y.; Chen, K. C.; Chiang, T. Y.; Lin, P. Y.; Tsai, T. D.; Chang, Y. C.; Guo, T. F.; Chen, P.; Wen, T. C.; Hsu, Y. J. Nickel Oxide Electrode Interlayer in  $CH_3NH_3PbI_3$  Perovskite/PCBM Planar-Heterojunction Hybrid Solar Cells. *Adv. Mater.* **2014**, *26*, 4107–4113.
- (30) Christians, J. A.; Fung, R. C. M.; Kamat, P. V. An Inorganic Hole Conductor for Organo-Lead Halide Perovskite Solar Cells. Improved Hole Conductivity with Copper Iodide. *J. Am. Chem. Soc.* **2014**, *136*, 758–764.
- (31) You, J.; Meng, L.; Song, T.-B.; Guo, T.-F.; Yang, Y.; Chang, W.-H.; Hong, Z.; Chen, H.; Zhou, H.; Chen, Q.; et al. Improved Air Stability of Perovskite Solar Cells via Solution-Processed Metal Oxide Transport Layers. *Nat. Nanotechnol.* **2016**, *11*, 75.
- (32) Punniyamurthy, T.; Velusamy, S.; Iqbal, J. Recent Advances In Transition Metal Catalyzed Oxidation of Organic Substrates with Molecular Oxygen. *Chem. Rev.* **2005**, *105*, 2329–2364.
- (33) Liu, J.; Li, Y.; Ke, J.; Wang, S.; Wang, L.; Xiao, H. Black NiO- $TiO_2$  Nanorods for Solar Photocatalysis: Recognition of Electronic Structure and Reaction Mechanism. *Appl. Catal., B* **2018**, *224*, 705–714.
- (34) Zhao, B.; Ke, X.-K.; Bao, J.-H.; Wang, C.-L.; Dong, L.; Chen, Y.-W.; Chen, H.-L. Synthesis of Flower-like NiO and Effects of Morphology on Its Catalytic Properties. *J. Phys. Chem. C* **2009**, *113*, 14440–14447.
- (35) Luo, B.; Liu, G.; Wang, L. Recent Advances in 2D Materials for Photocatalysis. *Nanoscale* **2016**, *8*, 6904–6920.
- (36) Huang, H. W.; Lin, J. J.; Fan, L. Z.; Wang, X. X.; Fu, X. Z.; Long, J. L. Heteroatomic Ni, Sn Clusters-grafted Anatase  $TiO_2$  Photocatalysts: Structure, Electron Delocalization, and Synergy for Solar Hydrogen Production. *J. Phys. Chem. C* **2015**, *119*, 10478–10492.
- (37) Perumal, A.; Shendre, S.; Li, M. J.; Tay, Y. K. E.; Sharma, V. K.; Chen, S.; Wei, Z. H.; Liu, Q.; Gao, Y.; Buenconsejo, P. J. S.; et al. High Brightness Formamidinium Lead Bromide Perovskite Nanocrystal Light Emitting Devices. *Sci. Rep.* **2016**, *6*, 36733.
- (38) Paul, M.; Pal, N.; Bhaumik, A. Mesoporous Nickel-Aluminum Mixed Oxide: a Promising Catalyst in Hydride-Transfer Reactions. *Eur. J. Inorg. Chem.* **2010**, 5129–5134.
- (39) Jing, L. Q.; Qu, Y. C.; Wang, B. Q.; Li, S. D.; Jiang, B. J.; Yang, L. B.; Fu, W.; Fu, H. G.; Sun, J. Z. Review of Photoluminescence Performance of Nano-Sized Semiconductor Materials and Its Relationships with Photocatalytic Activity. *Sol. Energy Mater. Sol. Cells* **2006**, *90*, 1773–1787.
- (40) Zheng, K. B.; Zidek, K.; Abdellah, M.; Messing, M. E.; Al-Marri, M. J.; Pullerits, T. Trap States and Their Dynamics in Organometal Halide Perovskite Nanoparticles and Bulk Crystals. *J. Phys. Chem. C* **2016**, *120*, 3077–3084.

(41) Liu, F.; Zhang, Y. H.; Ding, C.; Toyoda, T.; Ogomi, Y.; Ripolles, T. S.; Hayase, S.; Minemoto, T.; Yoshino, K.; Dai, S. Y.; et al. Ultrafast Electron Injection from Photoexcited Perovskite CsPbI<sub>3</sub> QDs Into TiO<sub>2</sub> Nanoparticles with Injection Efficiency Near 99%. *J. Phys. Chem. Lett.* **2018**, *9*, 294–297.

(42) Zhu, Z. L.; Bai, Y.; Zhang, T.; Liu, Z. K.; Long, X.; Wei, Z. H.; Wang, Z. L.; Zhang, L. X.; Wang, J. N.; Yan, F.; et al. High-performance Hole-Extraction Layer of Sol-gel-processed NiO Nanocrystals for Inverted Planar Perovskite Solar Cells. *Angew. Chem.* **2014**, *126*, 12779–12783.

(43) Xu, J.; He, S.; Zhang, H. L.; Huang, J. C.; Lin, H. X.; Wang, X. X.; Long, J. L. Layered Metal–Organic Framework/Graphene Nanoarchitectures for Organic Photosynthesis under Visible Light. *J. Mater. Chem. A* **2015**, *3*, 24261–24271.

(44) Lang, X. J.; Zhao, J. C.; Chen, X. D. Visible-Light-Induced Photoredox Catalysis of Dye-Sensitized Titanium Dioxide: Selective Aerobic Oxidation Of Organic Sulfides. *Angew. Chem., Int. Ed.* **2016**, *55*, 4697–4700.

(45) Li, X.-H.; Wang, X.; Antonietti, M. Solvent-Free and Metal-Free Oxidation of Toluene Using O<sub>2</sub> and Gc<sub>3</sub>n<sub>4</sub> with Nanopores: Nanostructure Boosts the Catalytic Selectivity. *ACS Catal.* **2012**, *2*, 2082–2086.